


Switching of the RKKY coupling on a topological crystalline insulating surface

Bui Dinh Hoi ^{*}

Faculty of Physics, *University of Education, Hue University*, Hue 530000, Vietnam



(Received 27 November 2023; accepted 7 May 2024; published 30 May 2024)

The ability to switch between ferromagnetic (FM) and antiferromagnetic (AFM) coupling in a material would increase the spintronic applications. To contribute, we focus on the Ruderman-Kittel-Kasuya-Yosida (RKKY) interaction between two magnetic impurities situated on the strained and gapped topological crystalline insulating SnTe(001) surface. By considering an in-plane strain and gap, we address the potential avenues for manipulating FM and AFM couplings in diverse adjustable manners. Our approach employs calculations based on retarded Green's functions in real space. For the strain effect on the intermediate impurity separations, we find that both uniaxial and biaxial strains switch all components of the RKKY coupling including XYZ-Heisenberg and symmetric, while the existence of a gap only switches the x component of the XYZ-Heisenberg coupling. By contrast, all components are switched with the strain and gap at long separations. Furthermore, we reveal that the switching process of the in-plane RKKY components can be distinctly modulated when the strain and gap coexist. To support the underlying physics of our numerical results, we provide explicit analytical expressions. These findings bear significance for magnetic data storage devices relying on topological materials.

DOI: [10.1103/PhysRevB.109.184441](https://doi.org/10.1103/PhysRevB.109.184441)

I. INTRODUCTION

One of the physical markers in spintronics [1,2] is the spin-spin exchange interaction (magnetic order) between magnetic impurities in a system [3–5]. Among various types of spin-spin interactions, the indirect Ruderman-Kittel-Kasuya-Yosida (RKKY) interaction between the magnetic spins, mediated by the itinerant electrons of the host material [6], is responsible for describing the oscillation between ferromagnetic (FM) and antiferromagnetic (AFM) couplings of spins [7]. It oscillates and decreases spatially with the impurity separation and, depending on the dimensionality of the host system, the decaying rates for the envelope of the oscillations differ: R^{-3} for three dimensions and R^{-2} for two dimensions [8–20]. External fields usually modulate the physical features of systems, e.g., it is well known that they tune the band gap in the electronic spectrum of a material. As the RKKY coupling depends on the electrons at the Fermi surface, it is sensitive to changes in the system.

Topological insulators are peculiar quantum systems in condensed-matter physics [21,22] as they propose a new phase of matter comprised of gapped bulk and intrinsic gapless surface states due to the strong spin-orbit coupling. The interesting gapless states are protected by the time-reversal symmetry [23–26]. When these states are protected by the crystal symmetries, weak topological insulators [27–30] and topological crystalline insulators (TCIs) such as SnTe and $\text{Pb}_x\text{Sn}_{1-x}\text{Te}$ [31–36] are introduced. In contrast to the strong topological insulators with an odd number of surface gapless (Dirac) states, TCIs possess an even number of Dirac states formed by C_2 and C_4 rotational symmetries. Such multiple

Dirac cones in TCIs are useful in multifunctional spintronic and valleytronic applications.

The research presented here is notably motivated by investigations into spin-spin interaction in the spintronics community, particularly in areas such as magnetic data storage devices [37]. In this active field, the pursuit of controlling magnetic orders remains a central theme. One of the fundamental open questions pertains to the adjustability of FM and AFM coupling of magnetic impurities.

Regarding the RKKY interaction in TCIs, Klier *et al.* [38] have focused on the correlation between the spin structure of the surface state and crystal field parameters, emphasizing tuning topological surface magnetism through bulk alloying. This is different from our work, which aims to provide ways to switch between FM and AFM coupling in TCIs for enhanced spintronic applications. In another work by Fertig *et al.* [39], magnetic ordering on the TCI's surface is investigated, probing topology and symmetry through RKKY interaction. The potential control of electron surface density is discussed, but the specifics of controlling the RKKY interaction for alternative magnetic orderings are not addressed. In the work by Ganjipour [40], a numerical argument on three types of RKKY interactions in TCIs is presented, but the focus is on numerically presenting such types of interaction, lacking discussion on tuning magnetic orderings. Significantly, Yarmohammadi and Cheraghchi [41] identify an effective low-energy RKKY interaction in doped TCIs, focusing on the z component of the Heisenberg interaction. However, they neglect the role of the inherent spin-orbit structure, which is present on the surface. Moreover, Cheraghchi and Yarmohammadi [42] study anisotropic ferroelectric distortion effects on RKKY interaction, emphasizing the complexity of the TCI's surface. While our work (see below for strain effect) and this work share similarities in lattice effects, our model

^{*}buidinhhoi@hueuni.edu.vn

demonstrates more reliable tuning of magnetic orderings through the modulation of Fermi velocities. This aspect differs from their use of distortion formalism to modulate the gap. The recent work by Yarmohammadi *et al.* [43], however, provides a comprehensive analysis of RKKY interaction on the TCI's surface with careful consideration of the spin-orbit structure, focusing on its detailed understanding and its influence on the quantum anomalous Hall effect, rather than tuning magnetic orderings.

Notably, none of the prior theoretical investigations of the RKKY interaction in TCIs have discussed potential methods for manipulating surface magnetism in these materials. Various mechanical and electrical strategies have been proposed and investigated to achieve such transitions [44–55], each exploiting distinct physical mechanisms. However, our study proposes the use of strain and gap for modulating surface magnetism in TCIs. As mentioned before, for the strain effect, we particularly consider the interaction of tensile and compressive strain on the lattice, which first manifests itself in the Fermi velocities and then modulates the RKKY interaction. This approach may be effective in the low-energy limit of the SnTe(001) surface, where the magnetic properties are closely tied to the behavior of electrons at the Fermi surface. For the gap effect, we choose to consider a universal description of the isotropically gapped SnTe(001) surface, regardless of the gap origin (e.g., substrate effects, electrical gating, nanoscale sculpturing, etc.). In a nutshell, we find that the FM and AFM couplings on the strain- and gap-induced TCI lattice drastically differ from the corresponding pristine ones.

The rest of this paper is organized as follows. In Sec. II, we briefly review the Hamiltonian model of pristine and strain- and gap-induced Dirac states on the SnTe(001) surface. In Sec. III, we present the RKKY theory and derive the necessary real-space Green's functions for the spin-spin interaction in the presence of strain and gap. We present the analytical and numerical results in Sec. IV, focusing on different possibilities for the strength of the strain and gap; phase diagrams highlight the switches between the FM and AFM couplings. Finally, we summarize the paper in Sec. V.

II. PRISTINE, STRAINED, AND GAPPED HAMILTONIAN OF SnTe(001) SURFACE

We start with a well-established continuum model [33–36,56,57] to describe the Dirac fermions on the SnTe(001) surface in which the effective electronic bands are formed by the p orbitals of sublattices Sn and Te and ground states are the admixture of spin-orbitally coupled states. This model, keeping the basic physics of the TCIs, separates the coupled coaxial Dirac cones at the low-energy limit: Two cones x and x' are located along the direction X - Γ - X of the projected surface Brillouin zone (SBZ) of the SnTe(001) surface, while two cones y and y' are located along the direction Y - Γ - Y , as shown in Fig. 1. The Hamiltonian of the X point in the absence of strain and a gap is simply given by (we set $\hbar = 1$) [41,42,56–58]

$$H_{x/x'}^{\text{pristine}} = \tilde{v}_x(k_x \mp x)\sigma_y - v_y k_y \sigma_x, \quad (1)$$

where $x = \sqrt{n^2 + \delta^2}/v_x$ is the location of the Dirac cone outside the SBZ along the X - Γ - X path and $\tilde{v}_x = \delta/x$ [58];

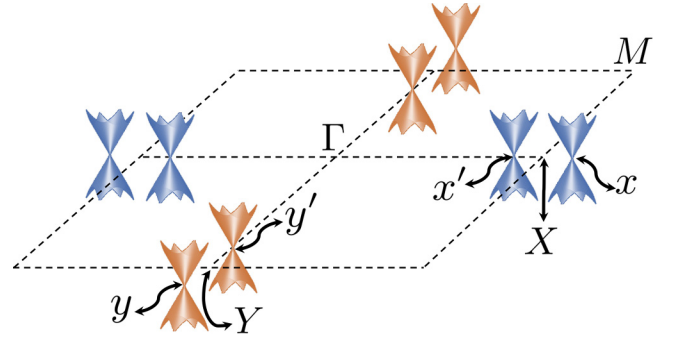


FIG. 1. Coaxial Dirac cones in the low-energy limit around the X and Y points of the pristine SnTe(001) surface, located at $x(x') = \pm\sqrt{n^2 + \delta^2}/v_x$ and $y(y') = \mp\sqrt{n^2 + \delta^2}/v_y$, where $v_x = 3.53 \text{ eV \AA}$ and $v_y = 1.91 \text{ eV \AA}$ refer to the Fermi velocities along the x and y direction, respectively. Furthermore, $n = 0.055 \text{ eV}$ and $\delta = 0.04 \text{ eV}$ denote intervalley scattering parameters. These gapless states are protected by the crystalline C_2 and C_4 rotational symmetries.

$n = 0.055 \text{ eV}$ and $\delta = 0.04 \text{ eV}$ [56,58] refer to the intervalley scattering parameters in the momentum space [58,59], while $v_x = 3.53 \text{ eV \AA}$ and $v_y = 1.91 \text{ eV \AA}$ refer to the Fermi velocities along the x and y direction, respectively [58,59]. Moreover, σ_x and σ_y are the sublattice Pauli matrices. It is worth noting that the above low-energy model is valid below the n parameter. As the values of $\tilde{v}_x \simeq 2.08 \text{ eV \AA}$ and v_y are close to each other, we neglect the weak anisotropy in the Hamiltonian and employ $\tilde{v}_x = v_y = v_F \simeq 2 \text{ eV \AA}$ for simplicity. Following the C_4 rotational symmetry, the other Hamiltonians for the Y point can be easily obtained. The energy spectrum of these Hamiltonians then is linear in the momentum space, as shown in Fig. 1. It should be noted that the basis set in the above Hamiltonian consists of $|1\rangle$ and $|2\rangle$, where $|1\rangle = [|\text{Te}, \uparrow\rangle + |\text{Sn}, \downarrow\rangle]/\sqrt{2}$ and $|2\rangle = [|\text{Sn}, \uparrow\rangle + |\text{Te}, \downarrow\rangle]/\sqrt{2}$, owing to the inherent spin-orbit coupling on the surface [60].

Next, we present the formula for the two-band Hamiltonian model discussed in Eq. (1) when the SnTe(001) surface is strained or gapped.

For the strain effect, we note that our strain theory is based on the modulation of orbital degrees of freedom, which have pronounced effects on the electronic properties of solids [61]. Thus, including a consideration of the orbital nature of bands, in our model, momentum space is shifted by the modulus of strain due to a lattice displacement \vec{u} with components $u_{\ell j} = (\partial_{\ell} u_j + \partial_j u_{\ell})/2$, which is strain modulus along the $\{\ell, j\} \in \{x, y\}$ direction. Note that the shear terms u_{xy} and u_{yx} are neglected for simplicity. This can be incorporated into the momentum space through a strain-induced gauge field vector potential $\vec{A} = \vec{x} - x$, where \vec{x} is the new location of the Dirac cone in the presence of strain. The linear relationship between the spatial displacement \vec{u} and \vec{A} in the vicinity of the X point (i.e., for x and x' Dirac cones) is given by [62]

$$\vec{A} = (\epsilon_1 u_{xx} + \epsilon_2 u_{yy}, \epsilon_1 u_{yy} + \epsilon_2 u_{xx}), \quad (2)$$

implying that the shift in the momenta is $\tilde{k}_x = k_x + \epsilon_1 u_{xx} + \epsilon_2 u_{yy}$ and $\tilde{k}_y = k_y + \epsilon_1 u_{yy} + \epsilon_2 u_{xx}$, where $\epsilon_1 = 0.3 \text{ \AA}^{-1}$ and $\epsilon_2 = 1.4 \text{ \AA}^{-1}$ arise from the orbital nature of the strained

conduction and valence bands in scanning tunneling microscopy [61]. Therefore, Eq. (1) becomes (following $\tilde{v}_x = v_y = v_F$)

$$H_{x/x'}^{\text{strained}} = v_F[(\tilde{k}_x \mp x)\sigma_y - \tilde{k}_y\sigma_x]. \quad (3)$$

For the gap effect, we universally open a band gap at each Dirac cone, while ignoring detailing the specific mechanisms responsible for gap generation. By adopting this approach, we can underscore the significance of gap magnitude in our work and facilitate direct comparisons across various realizations of strained and gapped SnTe(001) surfaces. It has been well demonstrated that such a gap can be easily incorporated into the Dirac Hamiltonian as a momentum-independent mass operator, such that

$$H_{x/x'}^{\text{gapped}} = v_F[(k_x \mp x)\sigma_y - k_y\sigma_x] + \frac{\Delta_z}{2}\sigma_z, \quad (4)$$

where Δ_z denotes the gap size. Note that σ_z in the sublattice space represents the basis sets of hybridized sublattices denoted by $|1\rangle$ and $|2\rangle$.

Eventually, the dressed Hamiltonian by the strain and gap reads

$$H_{x/x'}(\tilde{k}, \Delta_z) = v_F[(\tilde{k}_x \mp x)\sigma_y - \tilde{k}_y\sigma_x] + \frac{\Delta_z}{2}\sigma_z. \quad (5)$$

In both a strain- and gap-induced SnTe(001) surface, C_4 symmetry gives the modulated Hamiltonians of the y and y' Dirac cones around the Y point (not shown here to avoid repetition).

III. RKKY COUPLING ON STRAINED AND GAPPED SnTe(001) SURFACE

In this section, we overview the RKKY theory between two magnetic impurities \tilde{S}_1 and \tilde{S}_2 mediated by host itinerant electron \tilde{s} dressed by strain and gap effects on the SnTe(001) surface [7]. In this theory, the magnetic moments are treated classically on the lattice sites \tilde{R}_1 and \tilde{R}_2 and the interaction Hamiltonian is given by $H_{\text{int}} = \mathcal{J} \sum_{i=1}^2 \tilde{S}_i \cdot \tilde{s}_i$, where \mathcal{J} is the bare coupling between the impurity and the electron. Thus, the ordinary second-order perturbation theory yields

$$H_{\text{RKKY}}^{\alpha\beta} = \mathcal{J}^2 \sum_{\ell,j} S_1^{\ell\alpha} \chi_{\ell j}^{\alpha\beta}(\tilde{R}) S_2^{j\beta}, \quad (6)$$

where lattice sites are labeled by α and β for Sn and Te sublattices in the square lattice of the SnTe (001) surface. While different directions are shown by $\{\ell, j\} = \{x, y, z\}$, $\tilde{R} = \tilde{R}_2 - \tilde{R}_1$ is the impurity separation. Moreover, $\chi_{\ell j}^{\alpha\beta}(\tilde{R})$ is the spin susceptibility stemming from the retarded Green's functions in the spin space [9–11, 63], given by

$$\chi_{\ell j}^{\alpha\beta}(\tilde{R}) = -\frac{2}{\pi} \text{Im} \int_{-\infty}^{E_F} dE \eta_{\ell j}^{\alpha\beta}(E, \tilde{R}), \quad (7)$$

where

$$\eta_{\ell j}^{\alpha\beta}(E, \tilde{R}) = \text{Tr} [\sigma_\ell G_{\alpha\beta}(E, \tilde{R}) \sigma_j G_{\beta\alpha}(E, -\tilde{R})], \quad (8)$$

and $E_F = 0$ is the Fermi energy at zero temperature since we do not consider any electronic doping effect.

In the retarded Green's functions, we have the spin contribution of sublattices due to the intrinsic spin-orbit coupling.

This is because the valence and conduction bands are formed by hybridized p orbitals of Sn and Te. Thereby,

$$G_{\alpha\beta}(E, \tilde{R}) = \begin{pmatrix} G_{\alpha\beta}^{\uparrow\uparrow}(E, \tilde{R}) & G_{\alpha\beta}^{\uparrow\downarrow}(E, \tilde{R}) \\ G_{\alpha\beta}^{\downarrow\uparrow}(E, \tilde{R}) & G_{\alpha\beta}^{\downarrow\downarrow}(E, \tilde{R}) \end{pmatrix}, \quad (9)$$

in which one should take into account all Dirac cones along the directions X - Γ - X and Y - Γ - Y on the SBZ of the (001) plane. By this, we have

$$G_{\alpha\beta}^{ss'}(E, \tilde{R}) = \frac{1}{\Omega_{\text{SBZ}}} \int d^2\tilde{k} e^{i\tilde{k}\cdot\tilde{R}} [e^{i\tilde{X}\cdot\tilde{R}} G_{\alpha\beta}^{ss'}(\tilde{k} + \tilde{X}, E) + e^{i\tilde{Y}\cdot\tilde{R}} G_{\alpha\beta}^{ss'}(\tilde{k} + \tilde{Y}, E)], \quad (10)$$

where \tilde{k} comes from the strain effect, $\{s, s'\} = \{\uparrow, \downarrow\}$, and Ω_{SBZ} is the area of the SBZ. Rewriting the above equation results in

$$G_{\alpha\beta}^{ss'} = e^{iX R_x} (e^{ix R_x} \mathcal{V}_{\alpha\beta}^{ss'} + e^{-ix R_x} \underline{\mathcal{V}}_{\alpha\beta}^{ss'}) + e^{iY R_y} (e^{iy R_y} \mathcal{W}_{\alpha\beta}^{ss'} + e^{-iy R_y} \underline{\mathcal{W}}_{\alpha\beta}^{ss'}), \quad (11)$$

where $R_x = R \cos(\varphi_R)$ and $R_y = R \sin(\varphi_R)$. By defining $E + io^+ = i\varepsilon$ for $o^+ \ll 1$, we make use of the relation $\mathcal{V}_{\alpha\beta}^{ss'}(\varepsilon, \tilde{R}) = \Omega_{\text{SBZ}}^{-1} \int_0^\infty \tilde{k} d\tilde{k} \int_0^{2\pi} d\varphi_{\tilde{k}} e^{i\tilde{k} R \cos(\varphi_{\tilde{k}} - \varphi_R)} \mathcal{V}_{\alpha\beta}^{ss'}(\tilde{k}, \varepsilon)$, where $\varphi_{\tilde{k}} = \tan^{-1}(\tilde{k}_y/\tilde{k}_x)$ and, around the X point, we have $\mathcal{V}_{\alpha\beta}^{ss'}(\tilde{k}, \varepsilon) = [i\varepsilon - H_x(\tilde{k}, \Delta_z)]^{-1}$ and $\underline{\mathcal{V}}_{\alpha\beta}^{ss'}(\tilde{k}, \varepsilon) = [i\varepsilon - H_{x'}(\tilde{k}, \Delta_z)]^{-1}$. We note that the effective strain effect is incorporated into the phase factor in the above integral and the angle between two impurities is dressed by the strain modulus such that $\tilde{\varphi}_R = \varphi_R + \theta_u$, where $\theta_u = \tan^{-1}(A_y/A_x)$, with $A_x = \epsilon_1 u_{xx} + \epsilon_2 u_{yy}$ and $A_y = \epsilon_1 u_{yy} + \epsilon_2 u_{xx}$.

Finally, for the x and x' Dirac cones, the real-space Green's function in the basis of hybrid states $|1\rangle = [|\text{Te}, \uparrow\rangle + |\text{Sn}, \downarrow\rangle]/\sqrt{2}$ and $|2\rangle = [|\text{Sn}, \uparrow\rangle + |\text{Te}, \downarrow\rangle]/\sqrt{2}$ [43] reads

$$\mathcal{V}_{11}(\varepsilon, \tilde{R}) = -\mathcal{C} [i\varepsilon + \frac{\Delta_z}{2}] K_0(\tilde{\varepsilon} R/v_F), \quad (12a)$$

$$\mathcal{V}_{12}(\varepsilon, \tilde{R}) = -\mathcal{C} \tilde{\varepsilon} e^{-i\tilde{\varphi}_R} K_1(\tilde{\varepsilon} R/v_F), \quad (12b)$$

$$\mathcal{V}_{21}(\varepsilon, \tilde{R}) = +\mathcal{C} \tilde{\varepsilon} e^{+i\tilde{\varphi}_R} K_1(\tilde{\varepsilon} R/v_F), \quad (12c)$$

$$\mathcal{V}_{22}(\varepsilon, \tilde{R}) = -\mathcal{C} [i\varepsilon - \frac{\Delta_z}{2}] K_0(\tilde{\varepsilon} R/v_F), \quad (12d)$$

where $\mathcal{C} = 2\pi/\Omega_{\text{SBZ}} v_F^2$, $\tilde{\varepsilon} = \sqrt{\varepsilon^2 + \Delta_z^2/4}$, and K is the modified Bessel function. Similar expressions can be obtained around the Y point following the C_4 symmetry.

From the above equations, it is evident that $\mathcal{V}_{11/22}(\varepsilon, -\tilde{R}) = \mathcal{V}_{11/22}(\varepsilon, \tilde{R})$ and $\mathcal{V}_{12/21}(\varepsilon, -\tilde{R}) = -\mathcal{V}_{12/21}(\varepsilon, \tilde{R})$. This simplifies the expressions for the RKKY Hamiltonian. After straightforward calculations, we find

$$H_{\text{RKKY}}^{\alpha\alpha, \nu}(\tilde{R}) = \sum_{\ell} J_{\ell}(\tilde{R}) S_1^{\ell} S_2^{\ell} + \nu J_{xy}(\tilde{R}) [S_1^x S_2^y + S_1^y S_2^x], \quad (13a)$$

$$H_{\text{RKKY}}^{\alpha\beta}(\tilde{R}) = J_x(\tilde{R}) S_1^x S_2^x - J_y(\tilde{R}) S_1^y S_2^y - J_z(\tilde{R}) S_1^z S_2^z, \quad (13b)$$

where $\nu = +1$ (-1) characterizes the sublattice Te and Sn when the magnetic impurities reside on the same sublattices

$\alpha\alpha = \text{TeTe}$ and SnSn in Eq. (13a). Due to the spin-orbit structure of the model, impurities on different sublattices in Eq. (13b) only change the sign of the exchange couplings along the y and z directions, and this in turn leads to zero in-plane exchange contribution. It should be noted that when the impurities reside on the center of the squares and bonds between nearest neighbors Sn and Te, one can easily extract the RKKY responses by mixing the responses of the same and different sublattices due to the translational symmetry on the square lattice of the SnTe(001) surface. For this reason, we only focus on J_x , J_y , J_z , and J_{xy} couplings, given by $[J_\ell(\vec{R}) = \tilde{J}_\ell(\vec{R})/\pi\mathcal{J}^2\mathcal{C}^2]$

$$\tilde{J}_x(\vec{R}) = \pi\mathcal{J}^2\mathcal{C}^2\xi(\vec{R})\text{Im}\int_{o^+}^{\infty}i d\varepsilon\tilde{\varepsilon}^2[K_0^2(\tilde{\varepsilon}R/v_F) + \cos(2\tilde{\varphi}_R)K_1^2(\tilde{\varepsilon}R/v_F)], \quad (14a)$$

$$\tilde{J}_y(\vec{R}) = \pi\mathcal{J}^2\mathcal{C}^2\xi(\vec{R})\text{Im}\int_{o^+}^{\infty}i d\varepsilon\tilde{\varepsilon}^2[K_0^2(\tilde{\varepsilon}R/v_F) - \cos(2\tilde{\varphi}_R)K_1^2(\tilde{\varepsilon}R/v_F)], \quad (14b)$$

$$\begin{aligned} \tilde{J}_z(\vec{R}) = & \pi\mathcal{J}^2\mathcal{C}^2\xi(\vec{R})\text{Im}\int_{o^+}^{\infty}i d\varepsilon\tilde{\varepsilon}^2[K_0^2(\tilde{\varepsilon}R/v_F) \\ & + K_1^2(\tilde{\varepsilon}R/v_F)] \\ & - \frac{\pi\mathcal{J}^2\mathcal{C}^2\Delta_z^2}{2}\xi(\vec{R})\text{Im}\int_{o^+}^{\infty}i d\varepsilon K_0^2(\tilde{\varepsilon}R/v_F), \end{aligned} \quad (14c)$$

$$\begin{aligned} \tilde{J}_{xy}(\vec{R}) = & \pi\mathcal{J}^2\mathcal{C}^2\xi(\vec{R})\text{Im}\int_{o^+}^{\infty}i d\varepsilon\tilde{\varepsilon}^2\sin(2\tilde{\varphi}_R) \\ & \times K_1^2(\tilde{\varepsilon}R/v_F), \end{aligned} \quad (14d)$$

where $\xi(\vec{R}) = \cos^2(x\tilde{R}_x) + \cos^2(y\tilde{R}_y) + 2\cos(x\tilde{R}_x)\cos(y\tilde{R}_y)\cos(\frac{\pi}{\sqrt{2}a}[\tilde{R}_x - \tilde{R}_y])$ is the intersection (cross talk) between all Dirac cones on the SnTe(001) surface, with the lattice constant $a \approx 6.3 \text{ \AA}$, $\tilde{R}_x = R\cos(\tilde{\varphi}_R)$, and $\tilde{R}_y = R\sin(\tilde{\varphi}_R)$. While J_ℓ couplings are the Heisenberg interactions, J_{xy} is an in-plane symmetric interaction originating from the symmetry breaking of the spin space in the presence of magnetic impurities. It is worth noting that our model and theory are valid for all directions φ_R and impurity separations R .

IV. RESULTS

Before starting the analysis of our results, we comment on the experimental feasibility of our model. It should be noted that the experimental evidence potentially supporting our work is found in the literature, specifically in the work by Tanaka *et al.* [34]. This study documents the experimental observation of SnTe exhibiting a TCI phase through angle-resolved photoemission spectra. The metallic surface states are confirmed to be protected by the mirror symmetry of the crystal. In their work, it was illustrated that the low-energy approximation of the electronic band structure for the separation of coaxial Dirac cones is similar to our schematic in Fig. 1. This approximation occurs roughly below 100 meV, aligning with the parameters controlling the correlations

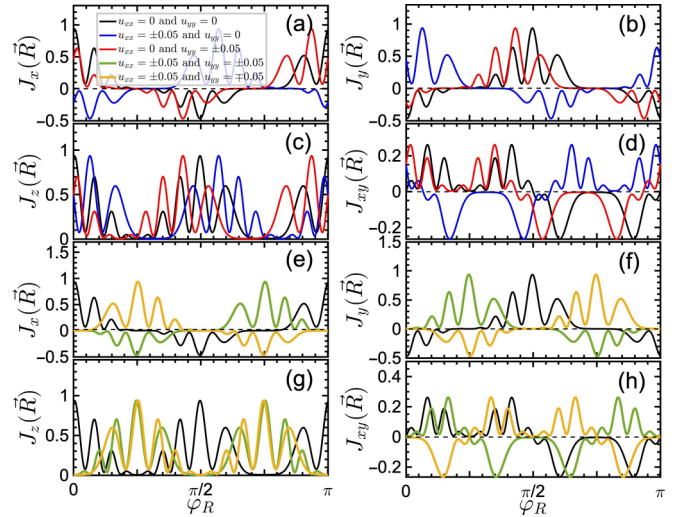


FIG. 2. (a)–(d) Uniaxial and (e)–(h) biaxial strain switching of the FM and AFM couplings in various RKKY components as a function of the direction φ_R at impurity separation $R/a = 10$ between two magnetic impurities. As soon as the system is strained, most RKKY couplings (except J_z) are modulated, associated with a sign change depending on φ_R .

between Dirac cones in our model, particularly $n = 55 \text{ meV}$. To maintain the validity of our model in the band structure, we set the upper limit of 10% for the strain modulus and gaps below 100 meV. These constraints ensure that the modulated bands are experimentally feasible in the presence of such strain and gap effects. Consequently, this experimental feasibility is expected to manifest in the observation of FM and AFM couplings in the RKKY interaction between two magnetic impurities on the SnTe (001) surface.

In our model, uniaxial strains are applied only with u_{xx} or u_{yy} , while biaxial strains deal with the application of both components. In what follows, we have rescaled couplings by a factor of 10^{-4} . Also, we employ $J_\ell > 0$ and $J_\ell < 0$ for the FM and AFM coupling, respectively. The significance of the RKKY interaction in spintronics lies not solely in its strength, but rather in its vital role in facilitating long-range magnetic interactions among localized spins. In many low-dimensional surfaces, the RKKY interaction may indeed be perceived as relatively weak in comparison to other forms of magnetic interactions. This characteristic arises from the nature of RKKY physics as an indirect exchange coupling mechanism, distinct from direct interactions. It is noteworthy that this attribute is not exclusive to TCIs, but is a broader phenomenon observed across various materials [43,64–66].

In Fig. 2, we focus on the strain effect on the RKKY components when the magnetic impurities reside on the SnTe(001) surface along different directions φ_R (we only present from 0 to π , while the same pattern repeats from π to 2π , which is not shown here) at fixed intermediate separation $R/a = 10$. The beating type of oscillations is evident, originating from the correlations of multiple surface Dirac cones, which is different from those of graphene and other two-dimensional materials [8,9,12]. This implies that multi-Fermi wave vectors generate the ultimate RKKY coupling, which can be easily understood from the cosine functions of $\xi(\vec{R})$.

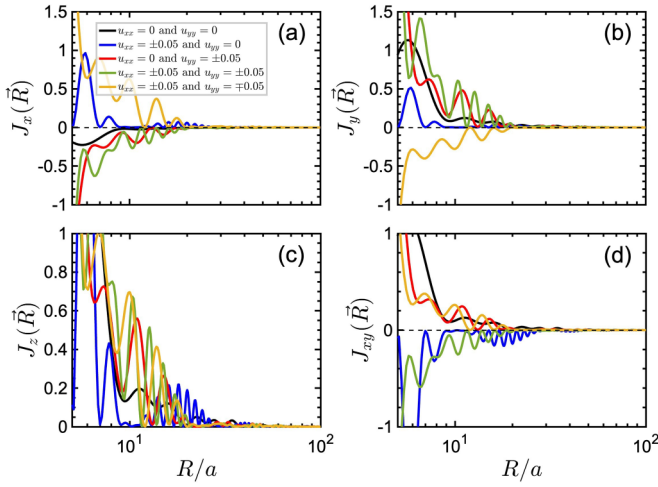


FIG. 3. The RKKY couplings as a function of the impurity separation R/a along the direction $\varphi_R = \pi/3$ for various strains. The strain does not affect the responses at long distances, while it switches the FM and AFM couplings at short and intermediate distances.

For the pristine (unstrained and gapless) structure, we have $u_{\ell\ell} = 0$ and $\Delta_z = 0$; therefore,

$$J_{x/y}(\vec{R}) = \xi(\vec{R})[1 \pm 3 \cos(2\varphi_R)] \frac{\pi^2 v_F^3}{32R^3}, \quad (15a)$$

$$J_z(\vec{R}) = \xi(\vec{R}) \frac{\pi^2 v_F^3}{8R^3}, \quad (15b)$$

$$J_{xy}(\vec{R}) = \xi(\vec{R}) \sin(2\varphi_R) \frac{3\pi^2 v_F^3}{32R^3}. \quad (15c)$$

In this case, all RKKY components show both FM and AFM couplings depending on φ_R ; see black lines in Fig. 2.

In the presence of uniaxial strain (see blue and red lines in Fig. 2), we still have the same expressions if we change $\varphi_R \rightarrow \tilde{\varphi}_R$ in Eq. (15); thus, $\{J_x, J_y, J_{xy}\}$ are switchable by strain due to cosine and sine functions, while J_z with FM coupling is robust against switching independent of the type of tensile or compressive strain. This is because, in Eq. (14c), there is no cosine and sine function of φ_R like the other three terms. For the oscillations in the correlation function $\xi(\vec{R})$, the uniaxial strain only shifts the period of oscillations. For the biaxial strain, however, more oscillations are observed, accompanied by substantial sign changes compared to the uniaxial one. Again, the J_z component maintains its initial FM coupling.

For the R dependency of RKKY coupling, Eq. (15) shows that the envelope of coupling decays as R^{-3} with fast (beating-type) oscillations in both short- and long-range impurity separations. For $\varphi_R = \pi/3$ (see black lines in Fig. 3), the inherent coupling of the J_x , J_y , J_z , and J_{xy} components is, respectively, AFM, FM, FM, and FM. As soon as we apply the uniaxial strain (both tensile and compressive) along the x direction, the AFM and FM coupling of J_x and J_{xy} is fully switched over the whole spatial spectrum [see Figs. 3(a) and 3(d)], while J_y and J_z remain unchanged [see Figs. 3(b) and 3(c)]. For the strain along the y direction, none of the components switch their intrinsic couplings; see red lines in

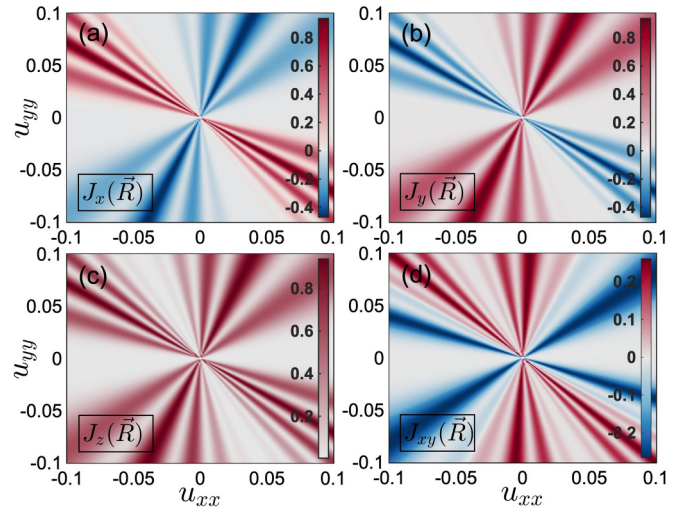


FIG. 4. Systematic study of the RKKY couplings when the SnTe(001) surface is strained at fixed $\varphi_R = \pi/3$ and $R/a = 10$. Switching AFM-FM and FM-AFM couplings effectively occurs for the biaxial strains following the spatial symmetries in Eq. (16).

Fig. 3. Turning to the biaxial strain, if u_{xx} and u_{yy} are both tensile or compressive (see the green line in Fig. 3), we only observe FM-AFM switching for the J_{xy} component. However, if one of u_{xx} and u_{yy} is tensile and another one compressive (or vice versa) (see yellow lines in Fig. 3), J_x and J_y are only switched. In the case of biaxial strain, the oscillations are much faster than uniaxial strain. In both uniaxial and biaxial strains, RKKY coupling for long separations between magnetic impurities is unaffected.

To systematically collect the information of the interplay between u_{xx} and u_{yy} , we provide a contour plot in Fig. 4 for an intermediate-range impurity separation $R/a = 10$ along the direction $\varphi_R = \pi/3$. For the J_x component, the significant changes in the magnetic orderings only emerge when biaxial strains are applied such that (i) AFM-FM coupling appears for tensile (compressive) u_{xx} and compressive (tensile) u_{yy} , and (ii) AFM coupling maintains for both tensile and compressive $u_{xx/yy}$. Due to the spatial symmetry of our model, we find

$$J_y(\vec{R}, \pm \vec{u}) = -J_x(\vec{R}, \pm \vec{u}), \quad (16a)$$

$$J_{x/y/xy}(\vec{R}, +\vec{u}) = -J_{x/y/xy}(\vec{R}, -\vec{u}). \quad (16b)$$

Still, no switching emerged for the J_j coupling.

Let us turn to the gap effect, where the main point is to break the symmetry between the Sn and Te sublattices of the SnTe square structure and hence to isotropically open a gap Δ_z in the band structure at the Dirac cones. A quick conclusion is that the RKKY couplings are symmetric with the gap as all components are even under $\Delta_z \rightarrow -\Delta_z$.

For the gapped structure at $\Delta_z \neq 0$, Eq. (14) can be separated into two terms. However, an analytical solution is not possible like the gapless phase and we have to apply some approximations to find approximate results for the short- and intermediate-/long-range impurity separations. It is necessary to mention that we use the following mathematical identity

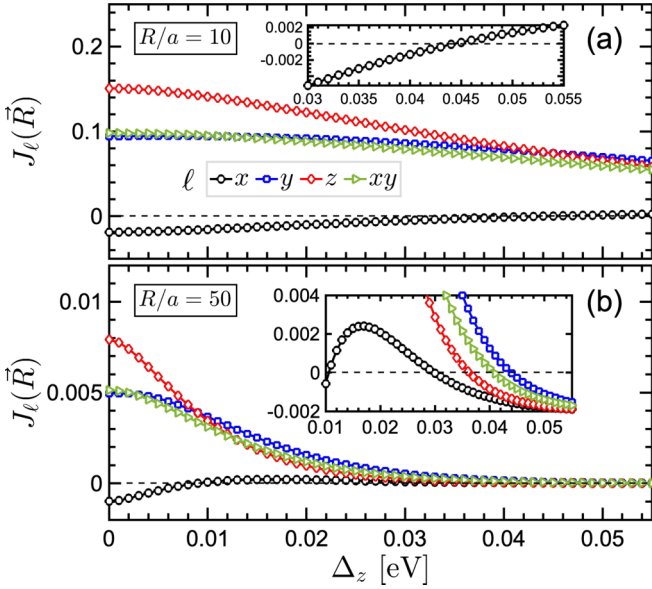


FIG. 5. The RKKY coupling on the SnTe(001) surface as a function of the gap at impurity separation (a) $R/a = 10$ and (b) $R/a = 50$ along the direction $\varphi_R = \pi/3$. For the intermediate-range separations in (a), only the AFM coupling of the J_x component is switched, while for the long-range separations in (b), all components are switched above $0.01 < \Delta_z < 0.03$ eV for J_x and $\Delta_z > 0.035$ eV for $\{J_y, J_z, J_{xy}\}$.

[67] for the short-range limit:

$$\int_0^\infty du u^{\alpha-1} K_\mu(cu) K_\nu(cu) = \frac{2^{\alpha-3}}{c^\alpha \Gamma(\alpha)} \Gamma([\alpha + \mu + \nu]/2) \times \Gamma([\alpha + \mu - \nu]/2) \times \Gamma([\alpha - \mu + \nu]/2) \times \Gamma([\alpha - \mu - \nu]/2). \quad (17)$$

Also, the following asymptotic expression for the modified Bessel functions is employed for the long-range limit:

$$K_\mu(u) \approx \sqrt{\frac{\pi}{2u}} e^{-u}. \quad (18)$$

Thus, applying the above expressions, we, respectively, find

$$J_\ell(\vec{R})|_{\Delta_z R/v_F \ll 1} \propto \frac{\xi(\vec{R})}{R^3}, \quad (19a)$$

$$J_\ell(\vec{R})|_{\Delta_z R/v_F \gg 1} \propto -\frac{\xi(\vec{R})}{R^{3/2}} \Delta_z^{3/2} e^{-\Delta_z R/v_F}. \quad (19b)$$

Thereby, the results should fall on top of each other at very short impurity separations, independent of the gap. Similar to the gapless structure, the envelope of coupling decays as R^{-3} with fast (beating-type) oscillations for very small impurity separations, while it decays as $R^{-3/2} e^{-R}$ for intermediate/large impurity separations.

In the case of intermediate distances at $R/a = 10$, which leads to $\Delta_z R/v_F > 1$, none of the components are switched up to $\Delta_z \approx 0.045$ eV; see Fig. 5(a). Above this critical gap, while the $\{J_y, J_z, J_{xy}\}$ components converge, the J_x component is switched. The sign switch is justified by Eq. (19b). The main origin is the intersection (cross talk) between all Dirac

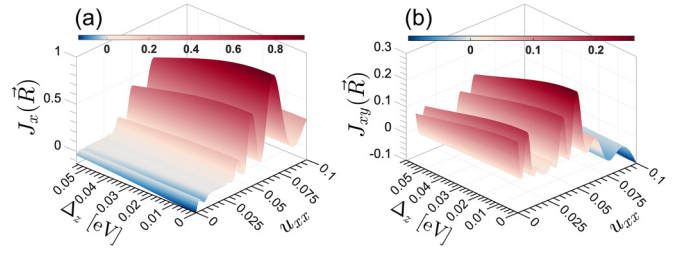


FIG. 6. The components (a) J_x and (b) J_{xy} of the RKKY coupling on the SnTe(001) surface as a function of the gap and the strain u_{xx} at $R/a = 10$, $u_{yy} = \pm 0.05$, and $\varphi_R = \pi/3$. Although the individual gap can switch J_x in this intermediate-range limit, strains $u_{xx} > 0.02$ make it nonswitchable, while nonswitchable J_{xy} with the gap becomes switchable for strain $u_{xx} > 0.06$.

cones on the SnTe(001) surface, i.e., $\xi(\vec{R})$. In the case of long impurity separations, however, alongside the gap dependency of response, which can be seen in Fig. 5(b), the couplings are also switchable at different critical gaps of $0.01 < \Delta_z < 0.03$ eV for J_x and $\Delta_z > 0.035$ eV for $\{J_y, J_z, J_{xy}\}$. Moreover, the exponential decay of RKKY coupling with the gap ($e^{-\Delta_z}$) is well justified. As a piece of useful information, let us argue that in turn, this implies that gap-induced RKKY involves fewer current densities compared to the pristine RKKY, which can be applicable in understanding the physics of the quantum anomalous Hall effect observed in magnetically doped topological insulators [68–71]. The underlying physics of magnetism switching induced by the gap involves several key principles and mechanisms, depending on the specific material and device architecture. However, in our material with strong spin-orbit coupling, the interaction between the electron's spin and its orbital motion can lead to the generation of an effective magnetic field when an electronic gap is generated at Dirac cones. This phenomenon, known as spin-orbit torque, can exert a torque on the magnetic exchange coupling between two magnetic impurities, leading to its reorientation. In most heavy metals or topological insulators such as our TCI, this is the main mechanism behind the switching process.

To gain further insights, we consider the simultaneous presence of strain and gap. We proceed with a plot of the J_x and J_{xy} couplings as a function of the gap Δ_z and strain u_{xx} at $R/a = 10$, $u_{yy} = \pm 0.05$, and $\varphi_R = \pi/3$ in Fig. 6. For J_y coupling and the other strain-type dependency of couplings, one would follow Eq. (16). In stark contrast to the absence of strain, RKKY coupling exhibits a different dependence on the gap when the strain is also present. It is straightforward to see that the AFM-FM switch at $0.01 < \Delta_z < 0.03$ eV for the J_x component does not survive above a critical strain $u_{xx} \approx 0.02$; see Fig. 6(a). On the other hand, the initial FM coupling of the J_{xy} component is switched to AFM at $u_{xx} > 0.06$; see Fig. 6(b). As a result of this, one would expect more adjustability when mechanical and electrical potentials are simultaneously applied in a magnetically doped TCI, which is useful information for spintronic applications.

V. SUMMARY

We have studied the RKKY interaction between two magnetic impurities on the SnTe(001) surface, as a well-known

topological crystalline insulator with spin-orbit coupling, to control the ferromagnetic/antiferromagnetic couplings. Using linear response theory based on retarded real-space Green's functions, we calculate the spin susceptibility by focusing on three regimes (short, intermediate, and long) for the impurity separation.

Our results illustrate that both uniaxial and biaxial strains with both tensile and compressive types can switch the ferromagnetic/antiferromagnetic couplings following the spatial symmetries in the model. We have also focused on the gap effect. While our analytical and numerical results show that there is an exponential decay for the RKKY coupling with the gap at intermediate- and long-range limits, RKKY coupling shows various antiferromagnetic-to-ferromagnetic switches, and vice versa, for the RKKY components. Finally, we have

shown that the application of strain and a gap at the same time leads to different results and the magnetism is differently adjustable on the SnTe(001) surface. We have found critical strains at which individual roles of the gap in switching the RKKY coupling are washed out.

The results presented here suggest that the control of RKKY coupling can be a promising method for fully switching magnetism in magnetic memory devices based on topological materials.

ACKNOWLEDGMENTS

This research is funded by Vietnam National Foundation for Science and Technology Development (NAFOSTED) under Grant No. 103.01-2021.68.

-
- [1] D. D. Awschalom and M. E. Flatté, Challenges for semiconductor spintronics, *Nat. Phys.* **3**, 153 (2007).
 - [2] R. Hanson, L. P. Kouwenhoven, J. R. Petta, S. Tarucha, and L. M. K. Vandersypen, Spins in few-electron quantum dots, *Rev. Mod. Phys.* **79**, 1217 (2007).
 - [3] I. Radu, K. Vahaplar, C. Stamm, T. Kachel, N. Pontius, H. A. Dürr, T. A. Ostler, J. Barker, R. F. L. Evans, R. W. Chantrell, A. Tsukamoto, A. Itoh, A. Kirilyuk, T. Rasing, and A. V. Kimel, Transient ferromagnetic-like state mediating ultrafast reversal of antiferromagnetically coupled spins, *Nature (London)* **472**, 205 (2011).
 - [4] J. H. Mentink, J. Hellsvik, D. V. Afanasiev, B. A. Ivanov, A. Kirilyuk, A. V. Kimel, O. Eriksson, M. I. Katsnelson, and T. Rasing, Ultrafast spin dynamics in multisublattice magnets, *Phys. Rev. Lett.* **108**, 057202 (2012).
 - [5] R. F. L. Evans, T. A. Ostler, R. W. Chantrell, I. Radu, and T. Rasing, Ultrafast thermally induced magnetic switching in synthetic ferrimagnets, *Appl. Phys. Lett.* **104**, 082410 (2014).
 - [6] C. Kittel, *Indirect Exchange Interactions in Metals Supported by the National Science Foundation* (Academic Press, San Diego, 1969), pp. 1–26.
 - [7] T. Kasuya, A Theory of Metallic Ferro- and antiferromagnetism on Zener's model, *Prog. Theor. Phys.* **16**, 45 (1956); K. Yosida, Magnetic properties of Cu-Mn alloys, *Phys. Rev.* **106**, 893 (1957); M. A. Ruderman and C. Kittel, Indirect exchange coupling of nuclear magnetic moments by conduction electrons, *ibid.* **96**, 99 (1954).
 - [8] S. Saremi, RKKY in half-filled bipartite lattices: Graphene as an example, *Phys. Rev. B* **76**, 184430 (2007).
 - [9] A. M. Black-Schaffer, RKKY coupling in graphene, *Phys. Rev. B* **81**, 205416 (2010).
 - [10] M. Sherafati and S. Satpathy, RKKY interaction in graphene from the lattice Green's function, *Phys. Rev. B* **83**, 165425 (2011).
 - [11] M. Sherafati and S. Satpathy, Analytical expression for the RKKY interaction in doped graphene, *Phys. Rev. B* **84**, 125416 (2011).
 - [12] V. K. Dugaev, V. I. Litvinov, and J. Barnas, Exchange interaction of magnetic impurities in graphene, *Phys. Rev. B* **74**, 224438 (2006).
 - [13] O. Roslyak, G. Gumbs, and D. Huang, Gap-modulated doping effects on indirect exchange interaction between magnetic impurities in graphene, *J. Appl. Phys.* **113**, 123702 (2013).
 - [14] M. Shiranzaei, F. Parhizgar, J. Fransson, and H. Cheraghchi, Impurity scattering on the surface of topological-insulator thin films, *Phys. Rev. B* **95**, 235429 (2017).
 - [15] M. Shiranzaei, J. Fransson, H. Cheraghchi, and F. Parhizgar, Nonlinear spin susceptibility in topological insulators, *Phys. Rev. B* **97**, 180402(R) (2018).
 - [16] M. Shiranzaei, H. Cheraghchi, and F. Parhizgar, Effect of the Rashba splitting on the RKKY interaction in topological-insulator thin films, *Phys. Rev. B* **96**, 024413 (2017).
 - [17] M. Ke and W.-K. Tse, Impurity states and indirect exchange interaction in irradiated graphene, *Phys. Rev. B* **106**, 075424 (2022).
 - [18] M. M. Asmar and W.-K. Tse, Interlayer RKKY coupling in bulk Rashba semiconductors under topological phase transition, *Phys. Rev. B* **100**, 014410 (2019).
 - [19] M. Ke, M. M. Asmar, and W.-K. Tse, Nonequilibrium RKKY interaction in irradiated graphene, *Phys. Rev. Res.* **2**, 033228 (2020).
 - [20] M. M. Asmar and W.-K. Tse, Floquet control of indirect exchange interaction in periodically driven two-dimensional electron systems, *New J. Phys.* **23**, 123031 (2021).
 - [21] M. Z. Hasan and C. L. Kane, *Colloquium: Topological insulators*, *Rev. Mod. Phys.* **82**, 3045 (2010).
 - [22] X.-L. Qi and S.-C. Zhang, Topological insulators and superconductors, *Rev. Mod. Phys.* **83**, 1057 (2011).
 - [23] H. Zhang, C.-X. Liu, X.-L. Qi, X. Dai, Z. Fang, and S.-C. Zhang, Topological insulators in Bi₂Se₃, Bi₂Te₃ and Sb₂Te₃ with a single Dirac cone on the surface, *Nat. Phys.* **5**, 438 (2009).
 - [24] J. E. Moore and L. Balents, Topological invariants of time-reversal-invariant band structures, *Phys. Rev. B* **75**, 121306(R) (2007).
 - [25] A. P. Schnyder, S. Ryu, A. Furusaki, and A. W. W. Ludwig, Classification of topological insulators and superconductors in three spatial dimensions, *Phys. Rev. B* **78**, 195125 (2008).
 - [26] R. Roy, Topological phases and the quantum spin Hall effect in three dimensions, *Phys. Rev. B* **79**, 195322 (2009).
 - [27] L. Fu, C. L. Kane, and E. J. Mele, Topological insulators in three dimensions, *Phys. Rev. Lett.* **98**, 106803 (2007).

- [28] R.-J. Slager, A. Mesaros, V. Juričić, and J. Zaanen, The space group classification of topological band-insulators, *Nat. Phys.* **9**, 98 (2013).
- [29] F. Zhang, C. L. Kane, and E. J. Mele, Topological mirror superconductivity, *Phys. Rev. Lett.* **111**, 056403 (2013).
- [30] W. A. Benalcazar, J. C. Y. Teo, and T. L. Hughes, Classification of two-dimensional topological crystalline superconductors and Majorana bound states at disclinations, *Phys. Rev. B* **89**, 224503 (2014).
- [31] J. C. Y. Teo, L. Fu, and C. L. Kane, Surface states and topological invariants in three-dimensional topological insulators: Application to $\text{Bi}_{1-x}\text{Sb}_x$, *Phys. Rev. B* **78**, 045426 (2008).
- [32] L. Fu, Topological crystalline insulators, *Phys. Rev. Lett.* **106**, 106802 (2011).
- [33] T. H. Hsieh, H. Lin, J. Liu, W. Duan, A. Bansil, and L. Fu, Topological crystalline insulators in the SnTe material class, *Nat. Commun.* **3**, 982 (2012).
- [34] Y. Tanaka, Z. Ren, T. Sato, K. Nakayama, S. Souma, T. Takahashi, K. Segawa, and Y. Ando, Experimental realization of a topological crystalline insulator in SnTe, *Nat. Phys.* **8**, 800 (2012).
- [35] P. Dziawa *et al.*, Topological crystalline insulator states in $\text{Pb}_{1-x}\text{Sn}_x\text{Se}$, *Nat. Mater.* **11**, 1023 (2012).
- [36] S.-Y. Xu *et al.*, Observation of a topological crystalline insulator phase and topological phase transition in $\text{Pb}_{1-x}\text{Sn}_x\text{Te}$, *Nat. Commun.* **3**, 1192 (2012).
- [37] M. Ameziane, R. Rosenkamp, L. Flajšman, S. van Dijken, and R. Mansell, Electric field control of RKKY coupling through solid-state ionics, *Appl. Phys. Lett.* **122**, 232401 (2023).
- [38] N. Klier, S. Sharma, F. Rost, O. Pankratov, and S. Shallcross, Tuning topological surface magnetism by bulk alloying, *Phys. Rev. B* **100**, 075130 (2019).
- [39] H. Fertig, S. Reja, S. Zhang, and L. Brey, Probing topology and symmetry in topological crystalline insulators with magnetism, *Physica E* **114**, 113623 (2019).
- [40] S. H. Ganjipour, RKKY interaction in topological crystalline insulators, *Can. J. Phys.* **99**, 614 (2021).
- [41] M. Yarmohammadi and H. Cheraghchi, Effective low-energy RKKY interaction in doped topological crystalline insulators, *Phys. Rev. B* **102**, 075411 (2020).
- [42] H. Cheraghchi and M. Yarmohammadi, Anisotropic ferroelectric distortion effects on the RKKY interaction in topological crystalline insulators, *Sci. Rep.* **11**, 5273 (2021).
- [43] M. Yarmohammadi, M. Bukov, and M. H. Kolodrubetz, Non-collinear twisted RKKY interaction on the optically driven SnTe(001) surface, *Phys. Rev. B* **107**, 054439 (2023).
- [44] Y. Zhu, Y. F. Pan, L. Ge, J. Y. Fan, D. N. Shi, C. L. Ma, J. Hu, and R. Q. Wu, Separating RKKY interaction from other exchange mechanisms in two-dimensional magnetic materials, *Phys. Rev. B* **108**, L041401 (2023).
- [45] K. Kargeti, A. Sen, and S. K. Panda, Strain-induced electronic and magnetic transition in the $s = \frac{3}{2}$ antiferromagnetic spin chain compound LaCrS_3 , *Phys. Rev. B* **109**, 035125 (2024).
- [46] Z. Shen, S. Dong, and X. Yao, Manipulation of magnetic topological textures via perpendicular strain and polarization in van der Waals magnetoelectric heterostructures, *Phys. Rev. B* **108**, L140412 (2023).
- [47] A. Pillai, S. Goel, L. D. Anh, and M. Tanaka, Control of magnetic anisotropy by epitaxial strain in the n -type ferromagnetic semiconductor $(\text{In,Fe})\text{Sb}$, *Phys. Rev. B* **108**, 014421 (2023).
- [48] P. P. Abrantes, W. J. M. Kort-Kamp, F. S. S. Rosa, C. Farina, F. A. Pinheiro, and T. P. Cysne, Controlling electric and magnetic Purcell effects in phosphorene via strain engineering, *Phys. Rev. B* **108**, 155427 (2023).
- [49] T. Janssen, M. Gidding, C. S. Davies, A. V. Kimel, and A. Kirilyuk, Strain-induced magnetic pattern formation in antiferromagnetic iron borate, *Phys. Rev. B* **108**, L140405 (2023).
- [50] S. Rijal, C. Xu, and L. Bellaiche, Designing frustration in two-dimensional magnetic systems via the application of uniaxial strain, *Phys. Rev. B* **103**, 014442 (2021).
- [51] A. O. Leon, J. d'Albuquerque e Castro, J. C. Retamal, A. B. Cahaya, and D. Altbir, Manipulation of the RKKY exchange by voltages, *Phys. Rev. B* **100**, 014403 (2019).
- [52] B. Li, W.-X. Qiu, and F. Wu, Electrically tuned topology and magnetism in twisted bilayer MoTe_2 at $\nu_h = 1$, *Phys. Rev. B* **109**, L041106 (2024).
- [53] Y. Wang, N. Luo, J. Zeng, L.-M. Tang, and K.-Q. Chen, Magnetic anisotropy and electric field induced magnetic phase transition in the van der Waals antiferromagnet CrSBr, *Phys. Rev. B* **108**, 054401 (2023).
- [54] R. Rouzegar, A. L. Chekhov, Y. Behovits, B. R. Serrano, M. A. Syskaki, C. H. Lambert, D. Engel, U. Martens, M. Münzenberg, M. Wolf, G. Jakob, M. Kläui, T. S. Seifert, and T. Kampfrath, Broadband spintronic terahertz source with peak electric fields exceeding 1.5 MV/cm, *Phys. Rev. Appl.* **19**, 034018 (2023).
- [55] J. Pang, X. Niu, M. Zhang, Y. Tang, Y. Zhang, and L. Bellaiche, Electric-field-induced formation and annihilation of skyrmions in a two-dimensional magnet, *Phys. Rev. B* **108**, 134430 (2023).
- [56] J. Liu, W. Duan, and L. Fu, Two types of surface states in topological crystalline insulators, *Phys. Rev. B* **88**, 241303(R) (2013).
- [57] M. Ezawa, Valleytronics on the surface of a topological crystalline insulator: Elliptic dichroism and valley-selective optical pumping, *Phys. Rev. B* **89**, 195413 (2014).
- [58] M. Serbyn and L. Fu, Symmetry breaking and Landau quantization in topological crystalline insulators, *Phys. Rev. B* **90**, 035402 (2014).
- [59] Y. Okada *et al.*, Observation of Dirac node formation and mass acquisition in a topological crystalline insulator, *Science* **341**, 1496 (2013).
- [60] Y. J. Wang, W.-F. Tsai, H. Lin, S.-Y. Xu, M. Neupane, M. Z. Hasan, and A. Bansil, Nontrivial spin texture of the coaxial Dirac cones on the surface of topological crystalline insulator SnTe, *Phys. Rev. B* **87**, 235317 (2013).
- [61] D. Walkup, B. A. Assaf, K. L. Scipioni, R. Sankar, F. Chou, G. Chang, H. Lin, I. Zeljkovic, and V. Madhavan, Interplay of orbital effects and nanoscale strain in topological crystalline insulators, *Nat. Commun.* **9**, 1550 (2018).
- [62] E. Tang and L. Fu, Strain-induced partially flat band, helical snake states and interface superconductivity in topological crystalline insulators, *Nat. Phys.* **10**, 964 (2014).
- [63] E. Kogan, RKKY interaction in gapped or doped graphene, *Graphene* **02**, 8 (2013).
- [64] H.-J. Duan, Y.-J. Wu, M.-X. Deng, R.-Q. Wang, and M. Yang, Indirect magnetic signals in Weyl semimetals mediated by a single Fermi arc, *Phys. Rev. B* **107**, 165147 (2023).
- [65] K. Laubscher, C. S. Weber, M. Hünenberger, H. Schoeller, D. M. Kennes, D. Loss, and J. Klinovaja, RKKY interaction in one-dimensional flat-band lattices, *Phys. Rev. B* **108**, 155429 (2023).

- [66] K. Laubscher, D. Miserev, V. Kaladzhyan, D. Loss, and J. Klinovaja, RKKY interaction at helical edges of topological superconductors, *Phys. Rev. B* **107**, 115421 (2023).
- [67] A. Prudnikov, I. Brychkov, I. Brychkov, and O. Marichev, *Integrals and Series: Special Functions*, Integrals and Series (Gordon and Breach Science, London, 1986).
- [68] R. Yu, W. Zhang, H.-J. Zhang, S.-C. Zhang, X. Dai, and Z. Fang, Quantized anomalous Hall effect in magnetic topological insulators, *Science* **329**, 61 (2010).
- [69] C.-Z. Chang *et al.*, Experimental observation of the quantum anomalous Hall effect in a magnetic topological insulator, *Science* **340**, 167 (2013).
- [70] X. Kou *et al.*, Scale-invariant quantum anomalous Hall effect in magnetic topological insulators beyond the two-dimensional limit, *Phys. Rev. Lett.* **113**, 137201 (2014).
- [71] J. G. Checkelsky, R. Yoshimi, A. Tsukazaki, K. S. Takahashi, Y. Kozuka, J. Falson, M. Kawasaki, and Y. Tokura, Trajectory of the anomalous Hall effect towards the quantized state in a ferromagnetic topological insulator, *Nat. Phys.* **10**, 731 (2014).